Constraint from displacement data on magma flux at Merapi volcano, Java

François Beauducel & François-Henri Cornet

Institut de Physique du Globe de Paris, Dpt Seismology
beauducel@ipgp.jussieu.fr, **cornet@ipgp.jussieu.fr**

Edi Suhanto, Made Agung

Volcanological Survey of Indonesia
edi@vsi.dpe.go.id, **made@ipgp.jussieu.fr**

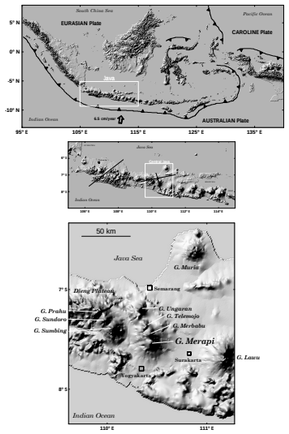

Photos. **(a)** View of Merapi from the North that reveals the strong asymetry of the edifice, and the high slopes of the volcano, reaching 57° near the summit. **(b)** The January 30 1992 lava dome. **(c)** November 22, 1994 pyroclastic flow that killed 69 people. Merapi presents an activity of quasi continuous extrusion of lava which forms a dome in a horse-shoe shaped crater. The dome is continuously and partially destroyed by avalanches and pyroclastic flows.

Figure 1. Location and geodynamical context of Mt. Merapi (2964 m). Merapi is a young strato-volcano located in Central Java, Indonesia, in a frontal subduction zone. Population of Yogyakarta (25 km from the summit) and arround is about 3 millions people, up to 500,000 are living directly on the flank of the volcano, above 500 m of elevation. Merapi is one of the « Decade Volcano » declared by the United Nations IDNDR program.

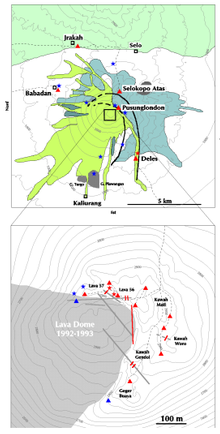

Figure 2. Geological setting and deformation network at Merapi. In red, benchmarks and stations installed for this study (GPS, tilts and extensometers). In blue, other collaborations with VSI (USA, Germany, Japan).

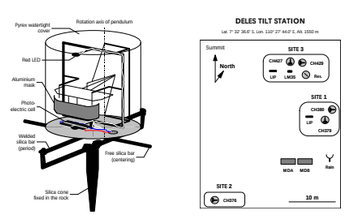

Figure 3. The Deles tilt station is located on the South-Est flank of Merapi (3 km from summit), on a compact and massive rock identified as a 5,000 years old pyroxene andesitic lava flow. The thickness reaches 200 m at some places and a few meters of young pyroclastic deposits cap it, constituting a thermal isolator, as compared with the massive rock below.
(a) Scheme of the horizontal pendulum *Compact Blum* made from welded silica.
(b) Sensor location (horizontal view) : 5 tiltmeters, 1 thermometer and 1 rainmeter.
(c) Vertical section of site 3 tilt installation.

Table 1. Deles tilt station sensor characteristics (range, digital resolution and RMS noise for 2-min and 1-day periods).

Sensor	Unit	Range	Resol.	2-Min σ	1-day σ
Tilt tan. CH379 (site 1)	µrad	155	$1.15\ 10^{5}$	0.0121	0.4106
Tilt rad. CH380 (site 1)	µrad	195	$5.40\ 10^{5}$	0.0099	0.3888
Tilt rad. CH376 (site 2)	µrad	248	$2.14\ 10^{5}$	0.0136	0.3163
Tilt tan. CH427 (site 3)	µrad	218	$2.00\ 10^{5}$	0.0117	0.7835
Tilt rad. CH429 (site 3)	µrad	578	$1.00\ 10^{5}$	0.0302	0.2693
Temp. LIP (site 1)	°C	100	$1.75\ 10^{4}$	0.0050	0.0837
Rainmeter (station)	mm	100 000	1		
Resistor bridge (site 3)	mV	10 000	$1.09\ 10^{3}$	0.0968	0.4471

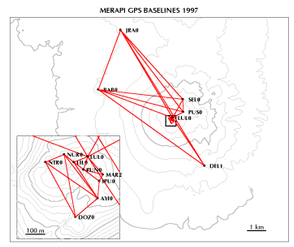

Figure 4. GPS baselines measured in November 1996, with 2 single-frequency receivers SERCEL NR101. The network was measured in 1993, 1994, 1995, 1996 and 1997.

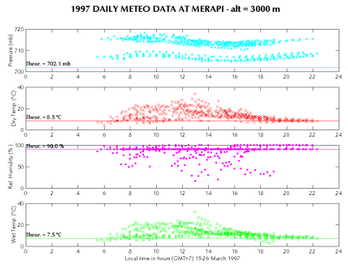

Figure 5. Meteorological data measured on the field during 1997 GPS campain. They have been reduced with respect to 3000-m elevation using standard vertical profiles of temperature, pressure and relative humidity, and are presented on a single day scale in local time. These data allow to determine a local meteo model of the troposphere for each time period of the GPS measurements, and are introduced in the double difference processing to compute baselines vectors. Introduction of meteo data is essential when the network covers large height differences as is the case for Merapi (1600 m).

Objectives

From deformation field analysis, we solve the boundary conditions common to the solid mechanics and the magma flux problems: internal structures geometry (plumbing system), pressure, stress and volume variations. The study also allows a better appraisal of monitoring measurements, thus helps hazard mitigation.

Methodology

We focus our study on Mt. Merapi, Java, Indonesia, a Decade Volcano with a quasi continuous activity: dome growth, explosions and pyroclastic flows. Deformation field measurement come from GPS network and multi-component continuous stations (tiltmeters and extensometers). Data are always validated by compensation to determine uncertainties. For modeling, we use three-dimensional elasto-static boundary elements [*Cayol & Cornet*, 1997] including topography, fractures and complex geometry sources. Inversion processes are used to estimate parameter evolution and model probability from observations.

Some conclusions

- Combination of high-precision tilt, displacements and topography constrains the modeling
- Evidence for a deep magma chamber at Merapi
- Evidence for fracture existence and their implications on the summit deformation field
- Compatibility of displacement observations and multi-phase seismic events: summit deformation field is controlled by magma flux
- Apparent elastic behaviour, but Young s modulus less than 1 GPa (possibly linear visco-elastic reality)
- Mass balance must include rock avalanches
- Identify potential rock slope problems

References

Cayol, V., and F.H. Cornet, 3D mixed boundary elements for elastostatic deformation field analysis, *Int. J. Rock Mech. Min. Sci.*, **34**, 275 287, 1997.

Beauducel, F., and F.H. Cornet, Collection and three-dimensional modeling of GPS and tilt data at Merapi volcano, Java, *J. Geophys. Res.*, 1998, in press.

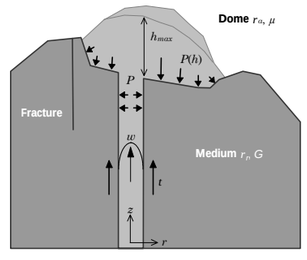

Figure 12. Types of source considered for the summit modeling of displacement field: dome weight effect on the crater floor, magma pressure in the duct and wall shear stress due to flux variation of viscous fluid. Computation of the dome weight effect for 1993-1994 period showed that this effect is negligeable on displacements.

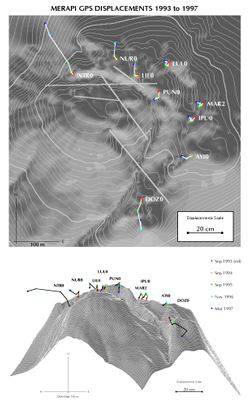

Figure 6. Cumulated displacements at the summit obtained by compensation of GPS baselines from 1993 to 1997. An important movement occured (about 40 cm) on the Northern part of the crater rim. Four « independent » zones separeted by fractures with different behavior are observed. **(a)** Horizontal view. **(b)** Vertical view from azimuth N145°E.

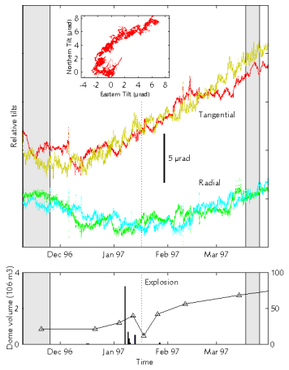

Figure 7. **(a)** Relative tilt signals at Deles between the 2 GPS campains (dashed zones): 2 radial and 2 tangential components. Inset plot shows the horizontal projection of the average motion of the tip of the normal to ground surface. **(b)** Dome volume estimation (solid line and triangles) and number of pyroclastic flows (bars) within the period. Dotted vertical line corresponds to the time of the dome explosion (January 17th, 1997).

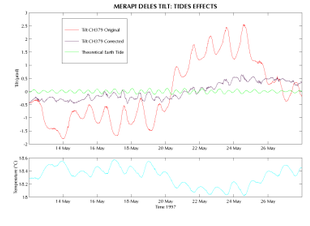

Figure 8. Example of tilt signal correction from temperature effects by a non-stationary linear method and comparison with theoretical earth tide variations computed for this location. This result validates the sensor coupling with the ground and the signal processing method used, which did not affect the complex tide signal included.

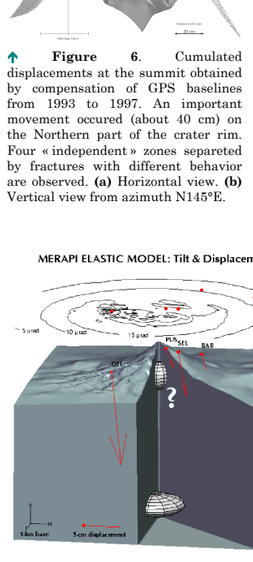

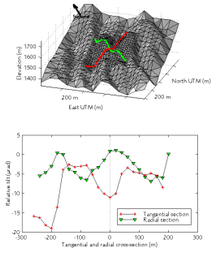

Figure 10. **(a)** 3-D mesh of topography around Deles tilt station. **(b)** Relative tilt computed along the cross-sections for the final ellipsoidal source solution. The tilt varies within ±1 µrad at ±20 m around the

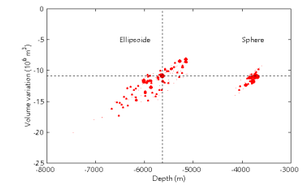

Figure 9. Monte-Carlo near-neighbor sampling inversion method (least squares best solution for 3D displacements and tilt vectors): projection of the model space in a 2-parameter plan (volume variation versus source depth). Dot size represents probability of each model (364 samples). Volume variation is well constrained but not the source shape and size.

Figure 11. 3-D deformation field modeling at Merapi on the 1996-1997 period: GPS displacements (red arrows), computed tilt field at the surface of the volcano (contour lines) and location of the tilt station (DEL). Deep magma chamber is deduced from both displacements and tilt observations. Because in elasticity, $\Delta P \propto \Delta V \propto$ displacements, we avoid the difficult task of Young s modulus estimation, and resolve only the volume variation of the source. Superficial magma chamber has been proposed from seismic observations but is not compatible with our deformation data. The computed volume variation is 3 times larger than the observed volume at the summit ($3.2 \pm 0.2\ 10^{6}$ m³).

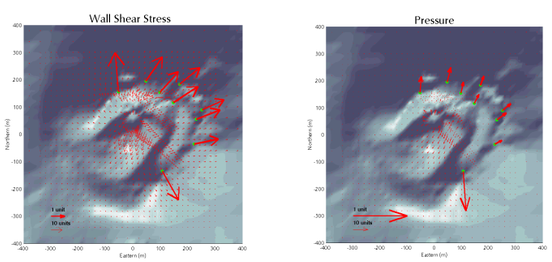

Figure 13. 3-D modeling of the summit deformations with 3 free fractures in the medium (horizontal view): displacement field (light arrows) and blow-up displacements on GPS points (heavy arrows). The displacement unit corresponds to 1 mm with a 1 MPa source and a Young s modulus of 30 GPa. **(a)** Results with wall shear stress in the duct. **(b)** Results with pressure source. A linear combination of the two sources effects allows to reproduce correctly the observed displacements pattern from 1993 to 1997 for all the points except for the North-West one (NTR), which probably exhibits an inelastic behavior.

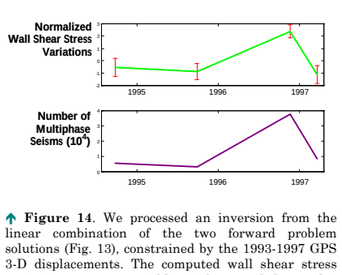

Figure 14. We processed an inversion from the linear combination of the two forward problem solutions (Fig. 13), constrained by the 1993-1997 GPS 3-D displacements. The computed wall shear stress variations are compatible with recorded « multi-phase » seismic events variations. Because the two observations are independent, this gives further support that these seismic events are related with shear stress release at the duct wall.